Arabian Journal of Chemistry (2021) **14**, 103069

King Saud University

Arabian Journal of Chemistry

www.ksu.edu.sa
www.sciencedirect.com

ORIGINAL ARTICLE

Polyditerpene acid from *Pinus koraiensis* pinecones inhibits the progression of hepatocarcinoma

Chao Xin, Yandong Zhang, Mengya Zhao, Zhenyu Wang *, Cuilin Cheng *

School of Chemistry and Chemical Engineering, Harbin Institute of Technology, Harbin 150090, China

Received 7 December 2020; accepted 7 February 2021
Available online 18 February 2021

KEYWORDS

Pinus koraiensis pinecones;
Cytotoxins;
Hexamer;
Apoptosis;
Hepatocarcinoma

Abstract The extracts of *Pinus koraiensis* pinecones have been proved to be highly cytotoxic to tumor cells, with ambiguous material basis of antitumor efficacy. In the present study, screening of compounds with antitumor activity was performed through successive applications of various purification technologies, accompanied with anticancer activity tracking. Futhermore, structures of target molecules were confirmed. In order to obtain highly active compounds, the lead compound dehydroabietic acid was chemically modified into its hexamer (DD2) by a simple method and its mechanisms for antitumor were explored *in vivo* and *in vitro* by some cell phenotype experiments, western blot, immunohistochemistry, TUNEL assay. Results showed that cytotoxins composed of 5-hydroxydehydroabietic acid, dehydroabietic acid, 15-hydroxy-7-oxodehydroabietic acid, 7α-hydroxydehydroabietic acid and inonotusic acid, exerted the synergistic antitumor effects against HepG2 cells. Especially, polymerization of multiple tricyclic skeletons effectively increased the cytotoxicity of dehydroabietic acid to tumor cells. Notably, DD2 exhibited stronger antitumor efficacy *in vitro* and *in vivo* mainly through the induction of G2/M cell cycle arrest and mitochondria apoptosis involving p53-Puma-Bcl-2/Bax axis. The analysis of liver / kidney function and HE staining demonstrated the no/low *in vivo* toxicity of DD2 to BALB/c nude mice. The findings will provide the theoretical reference to the discovery of new antitumor drugs and chemical modification of abietane diterpenoids.

1. Introduction

Cancer has greatly threatened human health, which is the second leading cause of death globally in 2017 (Cortes et al., 2020). In particular, hepatocellular carcinoma has the 3th highest mortality rate, due to its rapid progression, easy metastasis, poor efficacy and prognosis (IARC, 2020). Currently, the treatment strategies for hepatocellular carcinoma involve chemotherapy, radiotherapy, surgery, traditional Chinese medicine treatment, immunotherapy, targeted therapy, and so on (Batra et al., 2019) and chemotherapy is still the main-

* Corresponding authors at: 92 xidazhi street, nangang district, Harbin, China.
E-mail addresses: wzy219000@126.com (Z. Wang), ccuilin@hit.edu.cn (C. Cheng).

Peer review under responsibility of King Saud University.

Production and hosting by Elsevier

https://doi.org/10.1016/j.arabjc.2021.103069
1878-5352

stay of treatment modality. However, most chemotherapeutic drugs with poor targeting to tumor may cause damage or death of normal cells and show more serious side effects (Wei et al., 2020). In addition, some drugs such as therapeutic proteins, peptides and nucleic acids with poor stability exhibit worse therapeutic effects (Chung et al., 2014), limiting their application. More importantly, anticarcinogens are usually expensive and difficult to obtain (Cortes et al., 2020). Therefore, developing drugs with bargain price, high efficiency and low toxicity is urgently needed.

Over 60 species of *Pinaceae* plants are widely distributed all over of China, among them, 13 species are listed as medicinal plants by the *Chinese Pharmacopoeia*, with the medicinal parts including pinecones, pine nuts, pine needles (Hou et al., 2019). Pinecones, as the by-product of pine nuts, are one of the staple Chinese herbal medicine in China with long officinal history, beginning as outset in several medical masterpieces, such as *MING YI BIE LU* and *Supplement to Medica*, due to its excellent therapeutic effect on bronchitis, vitiligo and chronic low back pain. Recent studies have revealed various biological activities of pinecones: antivirus, antibacterial, antiinflammation, antitumor, and immune enhancement an so on (Zhang et al., 2019). Particularly, the antitumor effect of pinecones is attributed to various components including polysaccharide, polyphenols and terpenoids, which can improve immunity of tumor-bearing mice and induce mitochondrial apoptosis in tumor cells by activating of caspase 3, increasing the cellular reactive oxygen species (ROS) level, causing DNA damage, arresting cell cycle at G2/M phase and so on (Yi et al., 2016; Yi et al., 2017). In deed, pinecones are the low cost renewable materials of antitumor compounds and lead compounds. Unfortunately, most pinecones are only used as fuel or even discarded, resulting in a waste of resources and environmental pollution.

It has been found previously that 60% ethanol extract of *Pinus koraiensis* pinecones can effectively induce multiple tumor cell apoptosis in HT29, Hela, A549, SY5Y, especially, LOVO with an EC50 value of 0.317 ± 0.0476 mg/ml (Yi et al., 2015). Furthermore, HPLCMS suggests that chemical constituents mainly contained polyphenolic compounds (*e.g.* catechin, methyl quercetin, o-vanillin, luteolin and coronaric acid) (Yi et al., 2015). However, exact compounds responsible for antitumor effect have not been identified. Similar to some natural products, these antitumor ingredients in *Pinus koraiensis* pinecones are insufficient, and how to enhance drug efficacy is an urgent problem to be solved.

Herein, the research purposes are to identify the main antitumor compounds in pinecones, and to select the appropriate lead compound to enhance its activity through simple chemical modification, with the antitumor mechanism investigation of the modified compound *in vivo* and *in vitro*.

2. Materials and methods

2.1. Materials and reagents

Pinus koraiensis pinecones were provided by Yichun Hongxing District Forestry Bureau (Yichun, China) in October 2018. The whole pinecones without seeds or seed shell later were dried and then crushed into powder (800 μm).

Fetal bovine serum (FBS), High-glucose DMEM medium (4.5 g/l), penicillin–streptomycin were purchased from Thermo Fisher Scientific (China) Co., Ltd. Caspase 3, 8, 9, 12 activity assay kits (48 T), cell cycle detection kit (48 T), Annexin V-FITC/PI double staining apoptosis detection kit (48 T), cytochrome *c* assay kit (48 T), DNA damage assay kit (48 T) and reactive oxygen species assay kit (48 T) were obtained from Nanjing Jiancheng Bioengineering Institute. AFP quantitative detection kit (48 T) was obtained from Quanzhou Ruixin Biological Technology Co., LTD. Fluo-3 AM probe and ATP assay kit were purchased from Beyotime Biotechnology Co., Ltd. Primary antibodies as well as secondary antibodies were purchased from Proteintech Group, Inc. MTT and DMSO were obtained from Sigma-Aldrich Co., Ltd. in Shanghai. Other chemicals were commercially available from Shanghai Macklin Biochemical Co., Ltd.

2.2. Cell lines and culture

HepG2 cells were purchased from Shanghai Cell Bank (Shanghai Institute for Biological Science, Chinese Academy of Science,Shanghai, China). Cells were maintained in high-glucose DMEM (4.5 g/l), supplemented with 10% fetal bovine serum (FBS), 1% penicillin–streptomycin, incubated in a humidified atmosphere with 5% CO2 at 37 °C.

2.3. Cell viability assay (Zhang et al., 2019)

HepG2 cells (1×10^5 cells/mL) were seeded on 96-well microtitre plates and incubated overnight. The cells were treated with extract fractions or compounds (dissolved in 0.5% DMSO) in various concentrations (Fig. S2, 3, 10, 13), incubated for another 24 or 48 h. The relative cell viability was measured by standard MTT assay and EC50 values were calculated from the dose–response curves using CalcuSyn v2 Demo (Cambridge, UK).

2.4. Extraction and isolation with anti-cancer activity tracking

Various extraction and isolation protocols were indicated in Fig. S1. *Pinus koraiensis* pinecones (5 kg) were ultrasonicly extracted three times with 60% ethanol (solid–liquid ratio, 1 g : 30 ml) at 50 °C and 400 W for 1 h each time, and then the ethanol solution was recovered under reduced pressure at 55 °C . The obtained extract (800 g) was lyophilized, successively ultrasonicly extracted (50 °C, 400 W, 1 h) three times with ethyl acetate (EAC), and hot deionized water (solid–liquid ratio, 1 g : 20 ml). The total phenolic content was determined by Folin–Ciocalteu method using gallic acid as a standard according to the method reported in the literature (Yi et al., 2015). The ethyl acetate extract (200 g) was subjected to silica gel column chromatography [2.0 kg, chloroform–methanol, 1:0–9:1–4:1–7:3–3:2–5:5, v/v] to give fractions (Fr.) 1–6. Fr.2 (50 g) was purified multiple times by medium pressure preparative liquid chromatography system (MPLC, CombiFlash Rf 200, Teledyne ISCO, USA) [Silica gel, 40 μm, 20 g, 20 ml/min, 210 and 245 nm, chloroform–methanol, 1:0–4:1, v/v, 0–30 min] to give Fr. 1–4. Fr. 1 (30 g) was purified multiple times by MPLC (CombiFlash Rf 200, Teledyne ISCO, USA)

[ODS C18, 40 μm, 10 g, 15 ml/min, 245 nm, acetonitrile-H_2O, 25:75–100:0, v/v, 0–30 min] to give Fr. 1–4. Fr. 3 was purified multiple times by RP-HPLC (Gilson 281, Gilson, France) [Waters Symmetry Prep C18, 7 μm, 19*300 mm, 20 ml/min, 220 and 247 nm, acetonitrile-H_2O (0.1% TFA), 40:60–70:30–95:5–95:5–40:60–40-60, v/v, 0–20-20.5–24-24.1–26 min] give compound 1 (Co.1, 34 mg), compound 2 (Co.2, 97 mg), compound 4 (Co.4, 163 mg), compound 5 (Co.5, 175 mg). Every step of separation and purification was accompanied with anticancer activity tracking (MTT).

2.5. Synthesis of dehydroabietic acid derivatives

Dehydroabietic acid (80 mg), N-Hydroxysuccinimide (NHS, 245 mg) and 1-Ethyl-3-(3′-dimethylaminopropyl)carbodiimide (EDC, 408 mg) were dissolved in 50 ml N,N-Dimethylformamide (DMF), magnetic stirring for 30 min. And then, aminoacetaldehyde dimethyl acetal (224 mg) was added with magnetic stirring for 30 min under nitrogen atmosphere at room temperature. The resulting products were dialyzed (Mw cut-off: 200 Da) against deionized water (DI water) for 48 h, and the solids in the dialysis bag were collected and lyophilized. Then the solids dissolved in methanol were purified by preparative HPLC (RP-HPLC, Prep-HPLC), and lyophilized to give yellow powder (dehydroabietic acid derivative 1 ((1R,4aS)-N-(2,2-dimethoxyethyl)-7-isopropyl-1,4a-dimethyl-1,2,3,4,4a,9,10,10a-octahydrophenanthrene-1-carboxamide), 60 mg, named DD1). Dehydroabietic acid derivative 1 (50 mg) was dissolved in 50 ml DMF (containing 5 ml deionized water (DI water), 4 ml glacial acetic acid and 2 ml 6 M hydrochloric acid) and magnetically stirred for 48 h, keeping in dark, under nitrogen atmosphere at room temperature. The resulting products were dialyzed (Mw cut-off: 1000 Da) against DI water for 48 h, and the solids in the dialysis bag were collected and lyophilized. Then lyophilized solids were dissolved in methanol and purified by Prep-HPLC, and lyophilized to give white powder (dehydroabietic acid derivative 2 (Hexapoly((1R,4aS)-N-(2,2-dimethoxyethyl)-7-isopropyl-1,4a-dimethyl-1,2,3,4,4a,9,10,10a-octahydrophenanthrene-1-carboxamide)), 30 mg, named DD2). Structures of DD1 and DD2 were confirmed by 1H- and 13C NMR and FTICRMS (ESI^+; source accumulation, 0.020 sec; ion accumulation time, 0.200 sec; ranges (m/z) for DD1 and DD2 were respectively 50 ~ 450 and 50 ~ 2400.).

2.6. Structural characterization of main compounds

Compound composition of Fr.3 (obtained by ODS-C18-MPLC) was analyzed by ESI^+-HPLC-Orbitap Fusion (Orbitrap Fusion Lumos Tribrid, Thermo Scientific, USA) [Waters ACQUITY UPLC BEH C18, 1.7 μm, 2.1*100 mm, 0.8 ml/min, 220 and 247 nm, acetonitrile-H_2O (0.1% TFA), 30:70–100:0, v/v, 0–55 min]. The mass detection was carried out in the positive ion mode with the following settings: spray voltage, 3300 V; ion transfer tube temperature, 325 °C; vaporizer temperature, 275 °C; sheath gas velocity, 35 arb; auxiliary gas flow rate, 10 arb; sweep gas, 2 arb; full scan range, m/z 150 ~ 2000; RF lens, 30%; MSMS, m/z 50 ~ 2000; HCD collision energy, 30 ± 5%. 1H- and 13C NMR spectra of various compounds were collected by 600 MHz AVANCE III NMR spectrometer (Bruker, Germany) at 600 MHz for 1H NMR and 150 MHz for 13C NMR in different deuterated reagents. MS data of synthetic compound were obtained using FT ICR MS (9.4 T Solarix, Bruker, Germany).

2.7. In vitro synergism study of Co.1, Co.2, Co.4 and Co.5 (Chung et al., 2014)

The quantitative analysis of the combined therapeutic effects of Co.1, Co.2, Co.4 and Co.5 was performed using the combination index (CI) theorem of Chou-Talalay and CI was calculated by the following equation.

$$CI = \frac{(D)Co.1}{(D50)Co.1} + \frac{(D)Co.2}{(D50)Co.2} + \frac{(D)Co.4}{(D50)Co.4} + \frac{(D)Co.5}{(D50)Co.6}$$

where $(D)_{Co.1}$, $(D)_{Co.2}$, $(D)_{Co.4}$ and $(D)_{Co.5}$ were the concentrations of Co.1, Co.2, Co.4 and Co.5 used in combination to achieve 50% drug effect (24 h). $(D_{50})_{Co.1}$, $(D_{50})_{Co.2}$, $(D_{50})_{Co.4}$ and $(D_{50})_{Co.5}$ were the EC50 values for Co.1, Co.2, Co.4 and Co.5, independently (24 h).

2.8. Determination of caspase-3, 8, 9, 12, ATP and cytochrome c in the cytoplasm (Yi et al., 2016)

HepG2 cells were seeded in 6-well plates for overnight, incubated with various concentrations (0, 6, 8 μg/ml) of DD 2 for 24 h. The cells were then trypsinized and the total number of cells was counted. Caspase 3, 8, 9, 12 activity assay kits (Jiancheng), cytochrome *c* assay kit (Jiancheng) and ATP assay kit (Beyotime) were used to determined some apoptosis related indicators including activities of caspase-3, 8, 9, 12, cytochrome *c* in the cytoplasm and ATP content according to their respective instructions. Results were represented as the multiples of increase in enzyme activities or content compared with the control.

2.9. Cell cycle analysis (Zhang et al., 2019)

HepG2 cells were seeded in 6-well plates for overnight, incubated with various concentrations (0, 6, 8 μg/ml) of DD 2 for 24 h. The cells were then collected and stained, using cell cycle detection kit (Jiancheng), according to the manufacturer's instructions. The DNA content was determined by flow cytometry, and analyzed by CellQuest® software (BD Biosciences, USA).

2.10. Annexin V-FITC/PI staining (Zhang et al., 2019)

HepG2 cells were seeded in 6-well plates for overnight, incubated with various concentrations (0, 6, 8 μg/ml) of DD2 for 24 h. The cells were then collected and stained with annexin V-FITC and PI, incubated for 10 min in darkness, according to the manufacturer's instruction. Finally, the apoptotic cells samples were analyzed by flow cytometry (BD FACSCelesta, USA).

2.11. Measurement of intracellular reactive oxygen species (ROS) (Zhang et al., 2019; Yi et al., 2016)

HepG2 cells were seeded in 6-well plates for overnight, incubated with various concentrations (0, 6, 8 μg/ml) of DD2 for

24 h. And then, the cells were subsequently washed with PBS for three times, stained with 10 mM DCFH-DA for 30 min, washed with PBS again, collected and resuspended in PBS. Finally, the fluorescence intensity was measured with the fluorescence microscope (Olympus IX7, Japan), with excitation and emission wavelengths of 488 and 525 nm, respectively.

2.12. TEM characterization of mitochondrial morphology (Li et al., 2016)

HepG2 cells were seeded in 6-well plates for overnight, incubated with 6 μg/ml DD2 for 24 h. On the following day, cells were trypsinized, fixed, dehydrated, flatly embedded, cut into ultrathin flake and characterized using HT7650 TEM(Hitachi, Japan).The cells incubated with PBS were employed as the control.

2.13. Measurement of intracellular free Ca^{2+} (Zhang et al., 2019)

Fluo-3/AM probe was used to measure the intracellular free Ca^{2+} level in HepG 2 cells. The cells were treated with various concentrations (0, 6, 8 μg/ml) of DD2 for 24 h and collected. After that, the cells were loaded with 5 mM Fluo-3/AM for 60 min at room temperature, harvested, washed twice with PBS and analyzed by Flow cytometry (BD FACSCelesta, USA) .

2.14. Comet assay (Yi et al., 2016)

The DNA damage in HepG2 cells was evaluated using alkaline single cell gel electrophoresis. HepG2 cells were incubated with various concentrations (0, 6, 8 μg/ml) of DD2 for 24 h, collected and washed twice with cold PBS. And then, three-layer agarose gel containing cells was prepared. The cells underwent multiple treatments including lysis, DNA unwinding, single cell electrophoresis and staining according to the kit instructions. Finally, the samples were analyzed by fluorescence microscope (Olympus IX7, Japan).

2.15. Western blot analysis (Zhang et al., 2019; Wang et al., 2020)

Western blot assay was performed as described recently with minor modifications. Briefly, the harvested cells treated with various concentrations (0, 6, 8 μg/ml) of DD2 for 24 h were lysed in an ice-cold RIPA buffer containing protease inhibitors. After centrifugation at 12,000 rpm for 15 min, the concentration of soluble protein was determined by the BCA protein assay kit. Extracted protein boiled for 6 min was separated SDS-PAGE and transferred to PVDF membrane. Membranes were blocked, incubated with primary antibodies (p53, Puma, Bcl-2, Bax, caspase 3) overnight at 4 °C, and washed by TBST buffer. After that, the membranes were incubated with HRP-conjugated secondary antibody for 1 h at 37 °C, followed by a scan with Chemiscope 6000 Pro Imaging Analysis System (Clinx, Shanghai, China) and a analysis with Image J software.

2.16. In vivo therapy and evaluation of DD2 safety (Zhang et al., 2019)

Male BALB/c nude mice (four weeks) were selected as experimental model animals, which were purchased from Beijing Charles River Experimental Animal Technology Co., Ltd., (SCXK (Jing) 2016–0006, Beijing, China).

To prepare the tumor model, 1.0×10^7 HepG2 cells were suspended in fresh DMEM medium (50 μl) and subcutaneously injected into the right back region of BALB/c mice. When the tumor diameter reached about 8 ~ 10 mm, the tumor-bearing mice were divided into three groups randomly ($n = 3$, each group), and intratumoral (i.t.) injected with PBS only, DD2 dispersion only (5 mg/ml, 50 μl), or PTX dispersion only (5 mg/ml, 50 μl), respectively. Healthy mice were classified as blank group. After the treatment, tumor size and body weight of the each mice were measured every two days. The tumor growth inhibition rate (TGIR) was calculated according to the equation:

TGIR (%) = (1- G/G0) × 100%where G was tumor weight of mice in therapy groups (g), G0 was tumor weight of mice in the PBS group (g).

On day 16 after the injection, eye ball blood of each mouse was collected. Liver and renal function were determined by alanine aminotransferase (ALT), aspartate aminotransferase (AST), total bilirubin (TBIL), creatinine (Cr) and blood urea nitrogen (BUN) in serum using 7600 automatic biochemistry analyzer (Hitachi, Japan). In addition, the alpha-fetoprotein (AFP) in the serum was detected according to the kit instructions.

Tumors of the animals were collected and The apoptosis of tumor cells was analyzed via the terminal deoxynucleotide transferase (TdT)-mediated dUTP-biotin nickend labeling (TUNEL) assay. The expression of p53, Bax and Bcl-2 of each section was also analyzed (Li et al., 2019) by immunohistochemistry (ICH). The tissues of major organs of the mice including heart, liver, spleen, lung, kidney were stained by hematoxylin and eosin (HE) and imaged using an inverted fluorescence microscope (IX71, Olympus, Japan) for histology analysis.

2.17. Statistical analysis

Similar experiment was repeated three times. Data were expressed in the form of mean ± SD. Student's *t*-test was used for all statistical analysis between two groups while statistical analyses in which more than two groups were compared were performed using one-way ANOVA and Tukey post-hoc tests, using the IBM SPSS Statistics 23 software. $P < 0.05$ and $P < 0.001$ were accepted as significant and highly significant, respectively.

3. Results

3.1. *Isolation and identification of anticancer compounds from 60% ethanol extract of Pinus koraiensis pinecones*

60% ethanol extract of *Pinus koraiensis* pinecones as the antitumor active portion (Yi et al., 2015), could effectively inhibit HepG2 cell proliferation. Herein, the antitumor components

were continuously screened by various extraction and isolation approaches with anticancer activity tracking (Fig. S1). Lyophilized ethanol extract was successively extracted with EAC (*e.g.* terpenoids, polyphenols) and hot DI water (*e.g.* polyphenols, polysaccharides) (Xin et al., 2021). Total polyphenol contents of ethanol (Total), hot water (H_2O) and ethyl acetate (EAC) extracts were respectively 13.60%, 15.27%, 34.56% (mg/mg) (Fig. S2a), additionally, UV characteristic absorption wavelengths of EAC extract were 216 and 245 nm, with strongest absorption intensity (1 mg/ml) compared with Total and H_2O extracts, which were different from these of two typical polyphenol compounds (gallic acid and epigallocatechin gallate (EGCG)) (Fig. S2b). Particularly, EAC extract (500 μg/ml) showed strongest antiproliferative effects on HepG2 cells with the inhibition rate of 83% (Fig. S2c). These preliminary results indicated chemical compositions causing HepG2 cells apoptosis might not be polyphenols. Followed that, EAC extract was divided into 6 fractions using silica gel chromatography, and Fr.2 showed the most prominent inhibitory effects on HepG2 cells at the concentrations of 500 or 900 μg/ml (Fig. S2d). In addition, medium pressure liquid chromatography (MPLC) with different chromatography packings was employed to furtherly trace anticancer active sites, with the result that Fr.3 of MPLC (ODS-C18) exhibited the highest suppression efficiency on HepG2 cells (Fig. S3).

Furthermore, HPLC-Orbitap Fusion MSMS possessing characteristics of high resolution, sensitivity and accuracy was used to identify component compositions of Fr.3 of MPLC (ODS-C18), avoiding the drawback that more purification steps might cause loss of active compounds. HPLC-Orbitap Fusion MSMS showing Fr.3 of MPLC (ODS-C18) mainly contained 5 compounds (Fig. S4), whose feature fragments of first order (MS) and second order (MSMS) mass (m/z) were displayed in Table S1 and Fig. S5-9. Based on the MS fragment (m/z, 331.19012, $[M + H]^+$) and MSMS fragments (m/z, 313.20761, 285.17416, 271.19565, 227.14989, 145.06824), Co.3 was identified as 15-hydroxy-7-oxodehydroabietic acid according to the literature (Lee et al., 2017) (Fig. S4). For more accurate identification of the other 4 compounds, Fr.3 of MPLC (ODS-C18) was furtherly separated and purified, giving Co.1 (34 mg), Co.2 (97 mg), Co.4 (163 mg) and Co.5 (175 mg). Unfortunately, Co.3 was not successfully prepared, due to its lower content and resolution. Conclusively, NMR Spectroscopic Data (Table S2) and mass spectrometry data (Table S1) indicated the Co.1, Co.2, Co.4 and Co.5 were respectively 15-hydroxydehydroabietic acid, dehydroabietic acid, 7α-hydroxydehydroabietic acid and inonotusic acid (Liu et al., 2014) (Fig. S4). To our knowledge, this was the first report of the occurrence of an Co.5 in *Pinus koraiensis* pinecones. Interestingly, we found HPLC-Orbitap Fusion MSMS could effectively distinguish isomers (Co.1 and Co.4) (Table S1), which suggested this technology might provide a simple and reliable way to identify compounds in natural product.

3.2. Evaluation of anticancer activities for chemical constituents

Fig. S10 showed Co.1, Co.2, Co.4 and Co.5 could all effectively inhibit the proliferation of HepG 2 cells, with the EC50s of 154.2, 76.32, 164.01 and 129.50 μg/ml, respectively, higher than that of Fr.3 of MPLC (ODS-C18) (74.07 μg/ml). Based on the percentage values of compounds in Fr.3, obtained by HPLC-Orbitrap Fusion MSMS (Table S1), Co.1, Co.2, Co.4 and Co.5 were mixed, giving Fr.3+ (EC50, 80.32 μg/ml). The resulting CI of Fr.3 + was 0.63 (CI < 1), indicating the synergistic therapeutic effect between multiple compounds (Chou et al., 1994), more importantly, suggesting Co.1, Co.2, Co.4 and Co.5 as the main chemical compositions in Fr.3 could exert a synergistic anticancer effect. In addition, chemical structures of identified compounds revealed hydroxyl (Co.1, C-15; Co.4, C-7) and carbonyl (Co.5, C-7) exhibited negative anticancer effect on the compounds (Fig. S4).

3.3. Synthesis and activity evaluation of dehydroabietic acid derivatives

Although abietane-type diterpene compounds in *Pinus koraiensis* pinecones exhibit anticancer activities, whose inhibitory activities mainly depend on the structures of tricyclic diterpenes (Rao et al., 2008), these antitumor ingredients show insufficient efficacy. Consequently, the development of a simple and efficient method to synthesize dehydroabietic acid derivatives possessing stronger anticancer activities is of great significance (Rao et al., 2008). Recently, various chemical groups including thiourea, furan, amide, imidazole and sulfonylurea moieties have been introduced on dehydroabietic acid (Co.2) (Huang et al., 2013; Pertino et al., 2014; Huang et al., 2014; Li et al., 2019), greatly enhancing the antitumor capability of the unmodified compound. However, tedious steps, unstable reagents and harsh reaction conditions are usually required in these procedures. Consequently, the development of a simple and efficient method to synthesize dehydroabietic acid derivatives possessing stronger anticancer activities was of great significance. Herein, a simple synthesis method requiring mild conditions was proposed (Fig. 1), since these conventional reactions were easy to proceed, with higher yield of target compounds and fewer by-products: Firstly, DD1 was synthesized by the amidation reaction between carboxyl on dehydroabietic acid (Co.2) as lead compound and amino on aminoacetaldehyde dimethyl acetal, Secondly, DD2 was prepared by hydrolysis-condensation reaction between methoxy on DD1.

Structure elucidation of DD1 and DD2 was performed with NMR and FT ICR MS. Attributions of signals displayed in 1H and 13C NMR spectrum for DD1 were be confirmed (Table S3 and Fig. 2). The quasi-molecular ion peak at m/z 388.28078 $[M + H]^+$ (Fig. S11), confirming the molecular formula of DD1 was C24H37NO3. Signals attributable to C18-22 and related hydrogen atoms on aminoacetaldehyde dimethyl alcohol substituent (δ_C 181.8; δ_C 50.3, δ_H 3.39, dt, J 14.1 and 7.2 Hz; δ_C 157.9, δ_H 3.61, s; δ_C 55.1, δ_H 2.15, s; δ_C 55.1, δ_H 2.15, s) appeared, indicating DD1 was successfully synthesized. For DD2, its positive ESI-mass spectrum showed the quasi-molecular ion at m/z 2094.47841 $[M + H]^+$ accordingly to the molecular formula C134H192N6O13 (Fig. S11). 1D NMR spectrums of DD1 and DD2 in Fig. 2 with different magnifications all showed characteristic signals of abietane-type diterpenes (Co.2), suggesting tricyclic diterpene skeletons were unchanged in the hydrolysis-condensation reaction. In addition, signals belonging to methoxy (δ_C 55.1, δ_H 2.15, s), C19 and H19 (δ_C 50.3, δ_H 3.39, dt, J 14.1 and 7.2 Hz) were weakened or even disappeared, revealing substituents on

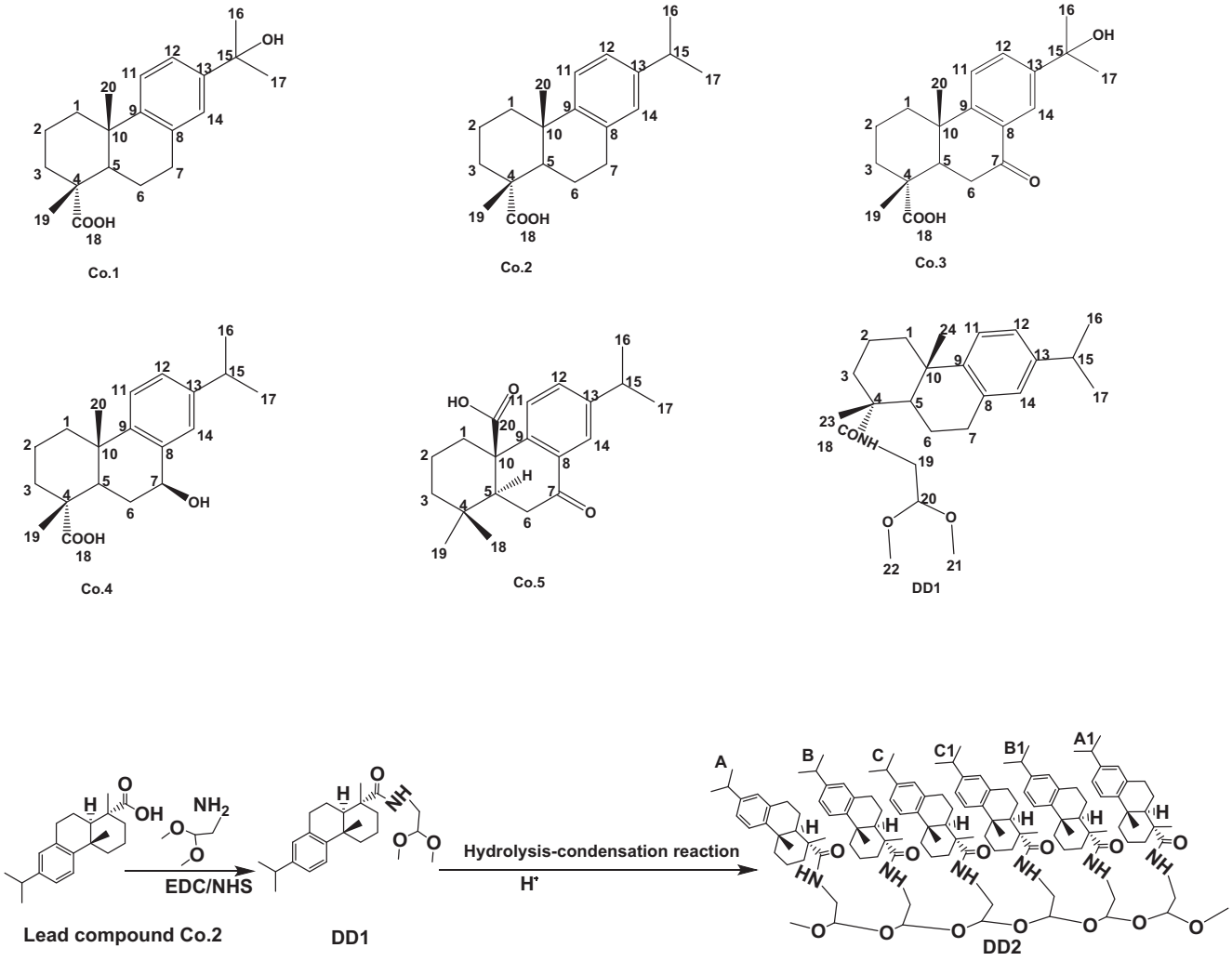

Fig. 1 Structures of related compounds.

DD1 participated in the reaction. However, changes of some signals such as aromatic signals could not be explained based on 1D NMR. Therefore, 2D NMR spectrums of DD2 including 1H–1H COSY, 1H–13C HSQC, 1H–13C HMBC were collected (Fig. S12). In the COSY spectrum, aromatic hydrogen signals of monomers in DD2 indicated the J^4 (H14 and H12) and J^3 (H12 and *H*11) couplings led to the peak splitting; some hydrogen signals on isopropyls and spiros could also be observed (δ_H 1.17, 1.16, 2.81, 2.82, 2.86, 2.85), especially, signals attributable to methoxy (δ_H 2.16) appeared, showing the presence of methoxys. In the HSQC spectrum, signals of δ 2.16/61.12, 2.13/61.11 were assigned to methoxy ends; signals of δ 3.52/85.9, 3.59/67.49 were respectively attributable to C-20 and H-20 in monomers (B/B1,C/C1); signals of δ 6.84/142.56, 6.87/142.61, 6.99/139.95, 7.17/140.20, 7.18/140.15 were attributable to *H*11-14 and C11-14 in different monomers. Signals of δ 1.33/173.77, 1.32/173.77, 3.58/172.73 in the HMBC spectrum suggested some amides existed in DD2. Briefly, synthesized DD2 proved to be the hexamer of DD1 (Fig. 1).

The MTT assays (Fig. S10 and Fig. S13) showed that the antitumor activity of dehydroabietic acid (Co.2, EC50 254.06 μM, 24 h) against HepG2 cells could be markedly improved by the introduction of aminoacetaldehyde dimethyl alcohol group (DD1, EC50 57.97 μM, 24 h), especially, polymerization of tricyclic diterpenes (DD2, EC50 4.65 μM, 24 h). It is important to note that DD2 exhibited the lowest EC50 values (4.65 μM, 24 h; 2.51 μM, 48 h), whose anticancer activity (against HepG2 cells) is even better than the commercial anticancer drug paclitaxel (PTX), with EC50s of 18.95 μM at 24 h or 12.81 μM at 48 h (Fig. S13), indicating preparation of dehydroabietic acid oligomers might be an effective method to discover new highly effective antitumor compounds.

3.4. DD2 induced cell cycle arrest and apoptosis in HepG2 cells

Suppressing tumor cell proliferation and inducing apoptotic death are efficient paths to hinder tumor progression. Majority of the antineoplastic agents exert their effects via arresting the cell cycle and / or triggering apoptosis (Duan et al., 2020). Drug-induced DNA damage signals could be transmitted to cell cycle regulatory genes, further leading to cell cycle arrest (Xu et al., 2017). To explore the mechanism of DD2 mediated cytotoxicity, the effects of DD2 on cell cycle distribution and apoptotic death were investigated by flow cytometry. As

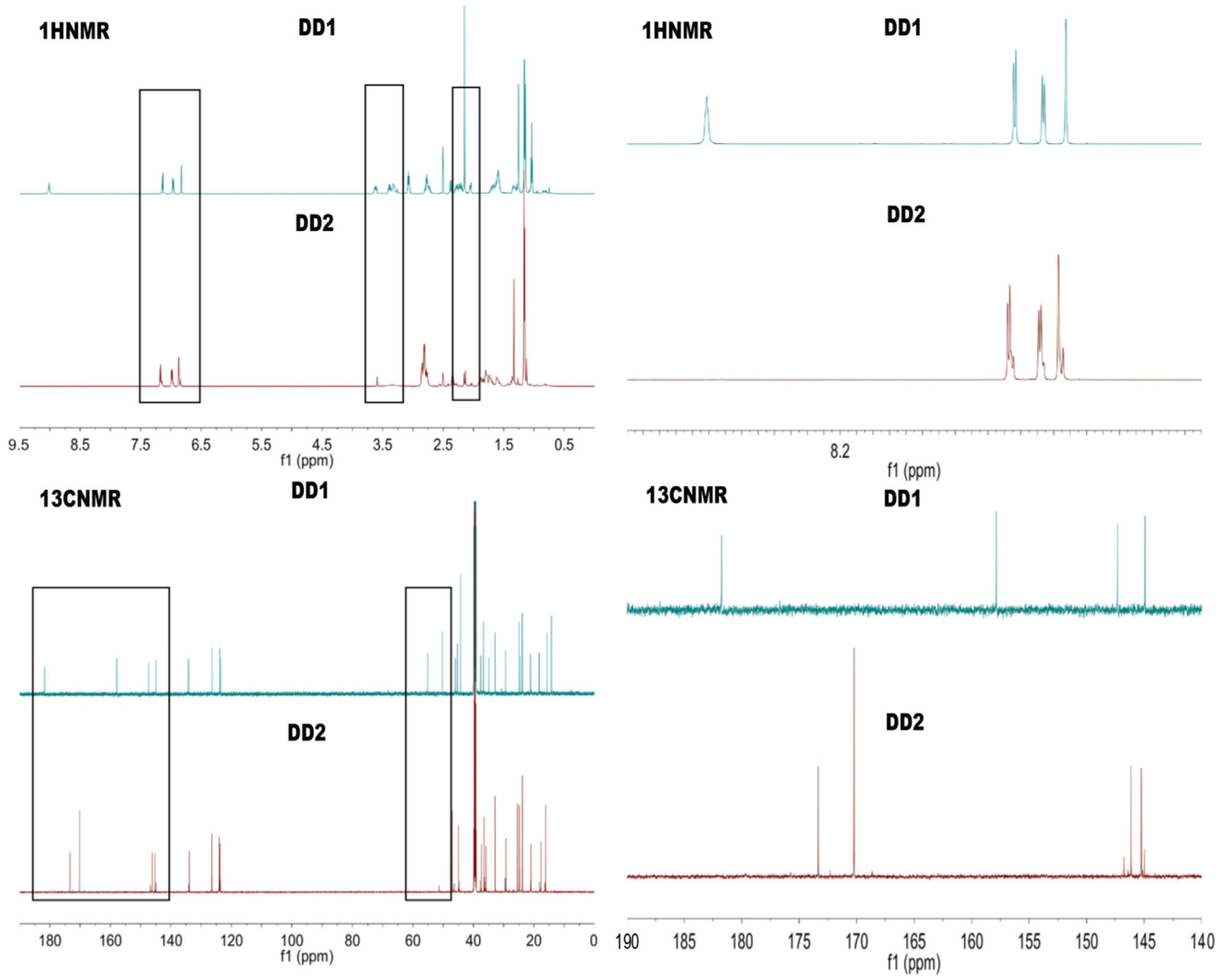

Fig. 2 1H NMR spectrums of DD1 and DD2.

shown in Fig. 3a-d, the exposure of HepG2 cells to DD2 (6 and 8 μg/ml) after 24 h, respectively caused 46.8% and 57.6% cells in G2/M phase as compared to control showing 17.2%. Inversely, G1 phase cell population was reduced remarkably (from 54.54% to 28.75% and 17.08%). Moreover, DD2-treated HepG2 cells had a significantly higher percentage total apoptotic cells (early and late apoptotic) in comparison to untreated cells in a concentration-dependent manner (Fig. 3e-h). Taken together, these results demonstrated DD2 could arrest HepG2 cells in the G2/M phase and trigger its apoptosis.

3.5. DD2 changed the caspase, cytochrome c and ATP in HepG2

Induction of tumor cell apoptosis is the basis of many cancer therapies (Takeda et al., 2007). Caspase family protease could trigger different apoptotic pathways such as death receptor, mitochondrial, and endoplasmic reticulum stress pathways (Takeda et al., 2007). Consequently, the activities of related caspases were respectively evaluated by kits and the results showed DD2 could significantly enhanced the activities of caspase 3, 8, 9 and 12 in a dose-dependent manner (Fig. 4d), indicating preliminarily three typical signal pathways mentioned above were all included in the apoptotic pathways triggered by DD2 (Mazumder, et al., 2008). During mitochondrial apoptosis, cytochrome *c* is released from the mitochondrial intermembrane space into the cytoplasm and the reduction in ATP content happens due to damaged mitochondrias (Garrido et al., 2006). Therefore, significant changes of ATP content and cytochrome *c* level in the cytoplasm caused by DD2 in different doses (Fig. 4d) suggested mitochondrial apoptosis was involved in apoptotic process initiated by this compound.

3.6. DD2 elevated intracellular reactive oxygen species levels (ROS) and caused DNA damage

Reactive oxygen species (ROS) at high concentrations could cause DNA damages such as DNA double strand breaks, and subsequently activate p53 and p53 upregulated modulator of apoptosis (Puma), which might further induce apoptosis (Magalhaes-Novais et al., 2019). Additionally, DNA damage is the inducing factor of cell cycle arrest (Xu et al., 2017).

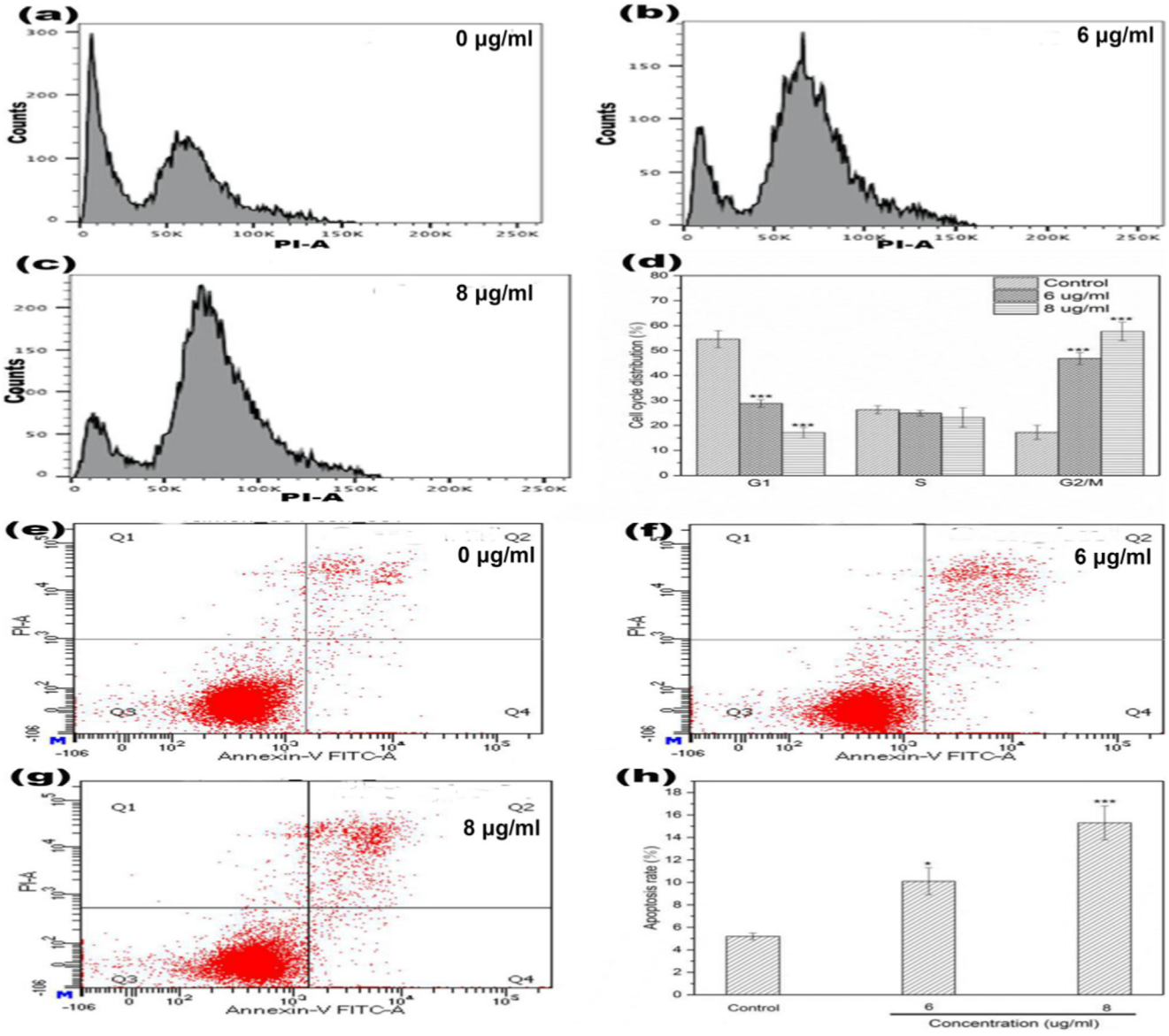

Fig. 3 a-h, Cell cycle and apoptosis analysis of HepG2 cells treated by DD2 for 24 h. d, h were respectively the numerical histogram of cell cycle distribution and the numerical histogram of apoptosis rate. Data represent the mean ± SD of three independent experiments. *P < 0.05, ***P < 0.001 *vs* untreated control cells.

Elevation of intracellular ROS levels and DNA damage in DD2-treated cells were investigated by the fluorescent probe DCFH-DA and comet assay. Fig. 4e-h showed intracellular ROS levels were significantly concentration-dependently elevated by DD2 as compared with control. PI staining displayed morphological changes of nuclei happened in HepG2 cells after treatment with DD2 (Fig. 4a-c). In DD2-untreated cells, nearly smooth and homogeneously stained nuclei with high-density DNA in comets head could be observed. After administration, obvious shrinkage or decomposition of nuclei and comet-like tails significantly different in length, generated by DNA migration could be easily discovered in HepG2 cells, implying occurrences of DNA damage. These results indicated DD2 elevated effectively intracellular production of ROS and further induced DNA damage, which is capable of triggering cell apoptotic death and cycle arrest.

3.7. DD2 increased levels of cytosolic calcium

Intracellular calcium overload represents dysregulation, probably caused by abnormal calcium release from endoplasmic reticulum to cytoplasm and calcium influx induced by ROS (Breckenridge et al., 2003; Giacomello et al., 2007), which might trigger endoplasmic reticulum stress (ER stress), mitochondrial dysfunction and final cell apoptosis (Breckenridge et al., 2003). ER stress induces apoptosis not only by directly activating the pro-apoptotic protein caspase 12 but also by activating cascades of pro-apoptotic proteins (*e.g.* caspase 9, 3, cytochrome *c*) to induce DNA damage (Yapasert, et al., 2020), the important trigger of mitochondrial apoptosis. In addition, excess calcium ions are ingested into mitochondria through mitochondrial calcium uniporter (MCU), causing eventually the increase of mitochondrial outer membrane per-

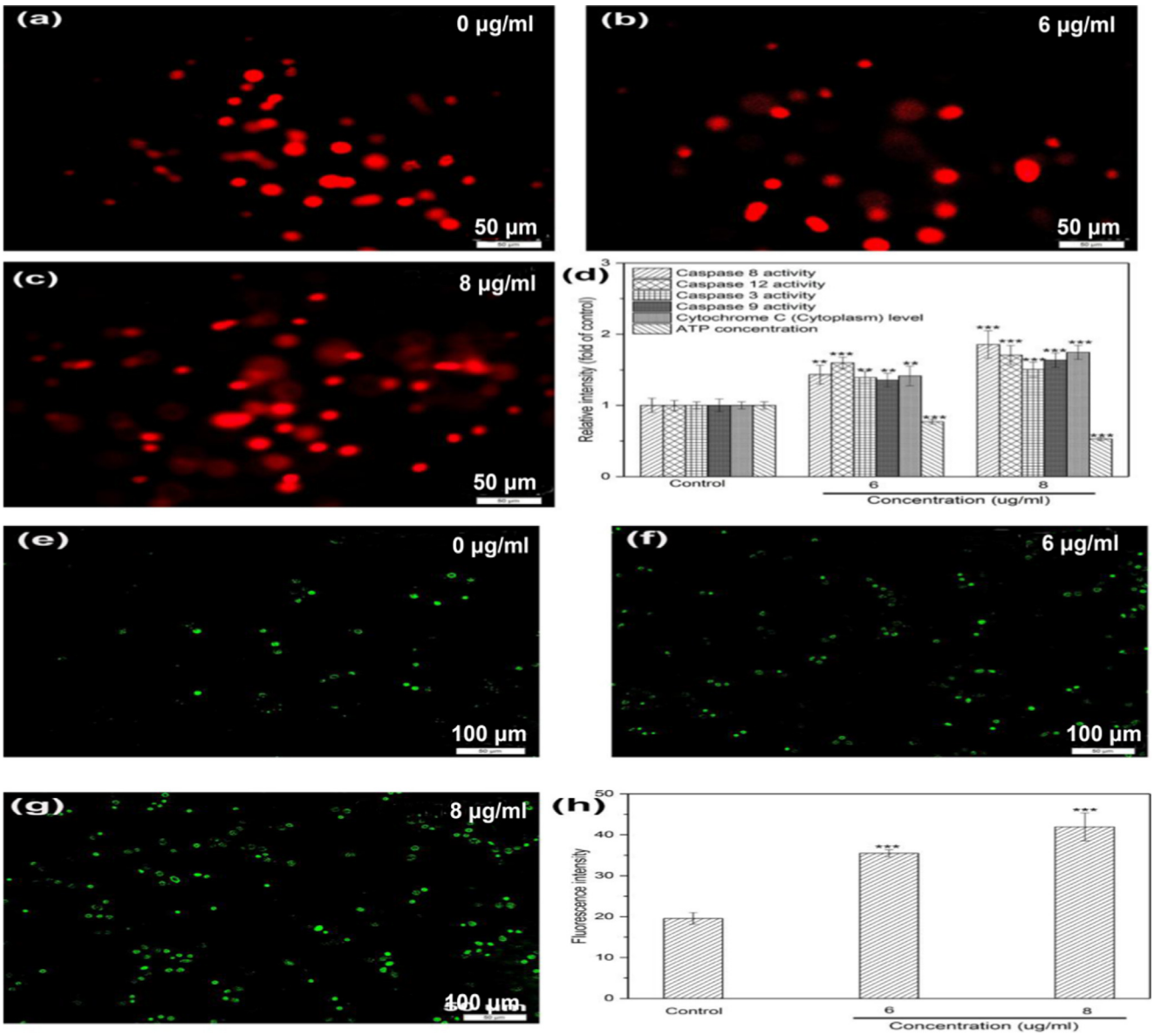

Fig. 4 Indicator anaysis of HepG2 cells treated by DD2 for 24 h. a-c, Fluorescence images of comet; d, Effect of DD2 on caspase activities, ATP concentration and cytoplasmic cytochrome *c* level in cells; e-h, Effect of DD2 on intracellular ROS. Data represent the mean ± SD of three independent experiments. $^{**}P < 0.01$, $^{***}P < 0.001$ *vs* untreated control cells.

meabilization (MOMP) and the release of pro-apoptotic factors (Giorgi, et al., 2012). Conclusively, calcium ion was one of the key regulators associated with mitochondrial apoptosis. To determine whether calcium ions were involved in the regulation of apoptosis induced by DD2, a fluorescent probe Fluo-3/AM was employed to monitor the changes of cytoplasmic calcium levels in HepG2 cells before and after administration. As was shown in Fig. 5a-d, treatment with DD2 resulted in a significant elevation of cytoplasmic calcium ion concentrations in a dose-dependent manner. The results suggested the elevation of calcium levels was closely related to DD2-induced apoptosis.

3.8. DD2 changed the mitochondrial morphology in HepG2 cells

Elevated ROS and cytoplasmic calcium ion levels might result in mitochondrial swelling and dysfunction followed by apoptosis. Our results have shown that DD2 could induce calcium overload and ROS production, therefore, TEM was applied to examine whether changes in mitochondrial morphology and ultrastructure happened.

The mitochondria of cells in the control group were numerous, evenly distributed and shaped in rod or long tube, and showed clear and neatly arranged crest with uniform matrix (Fig. 5e). In the cells treated with DD2, massive autophagosomes and lysosomes appeared in the cytoplasm and mitochondria with disorderly arranged crest were irregularly shaped, unevenly distributed. Particularly, mitochondrial vacuoles showed obvious degeneration and swelling (Fig. 5f), indicating mitochondrial structure was severely destroyed by DD2. The results revealed that mitochondrial disruption was included in apoptosis triggered by DD2.

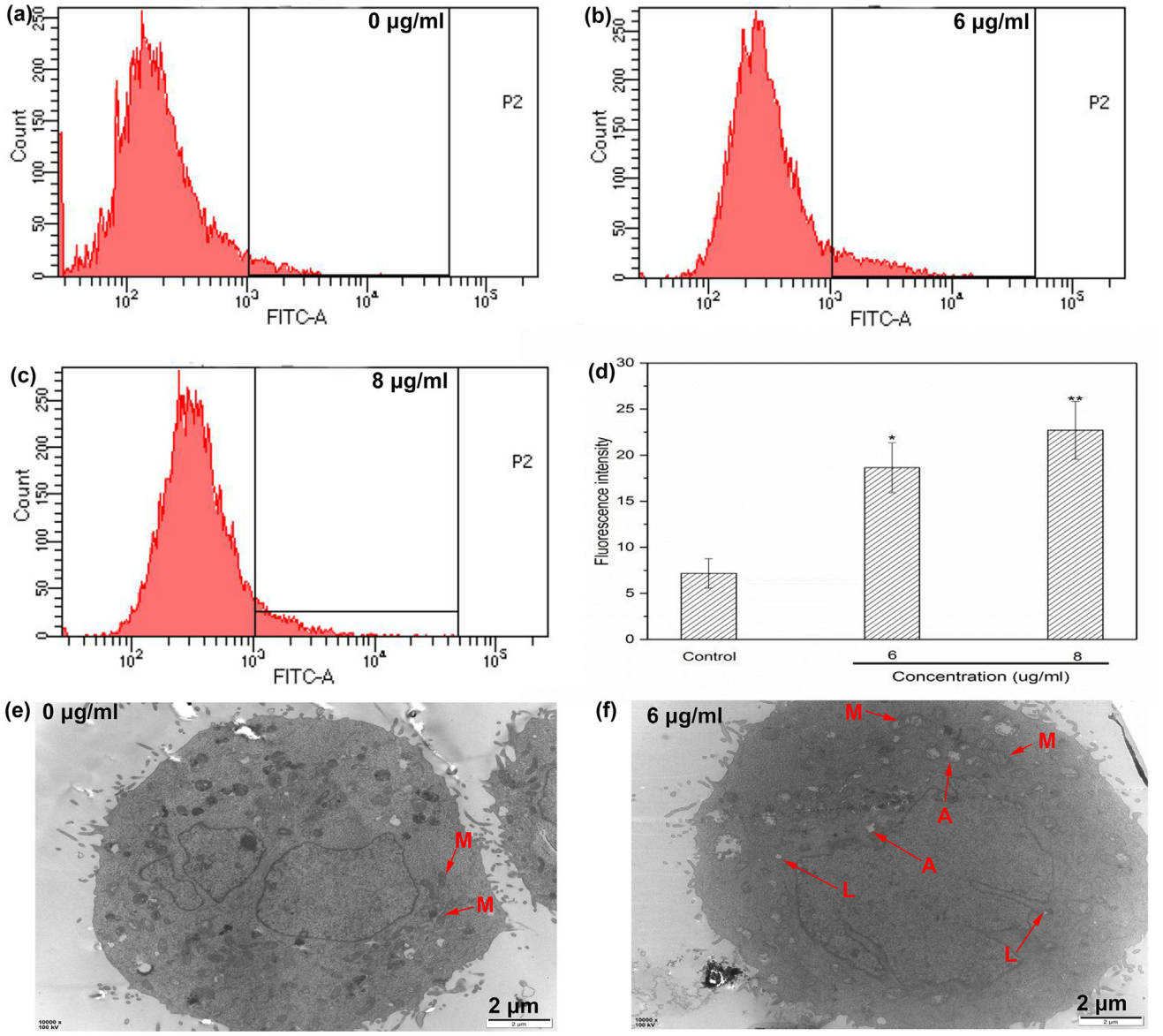

Fig. 5 a-d, Effect of DD2 on intracellular free calcium ion; e-f, TEM images of HepG2 cells before and after incubation with DD2 for 24 h, M, A and L refered to mitochondria, autophagosomes and lysosomes, respectively. Data represent the mean ± SD of three independent experiments. *P < 0.05,**P < 0.01 *vs* untreated control cells.

3.9. DD2 induced mitochondrial apoptosis in HepG2 cells through P53/Puma pathway

Cell phenotype experiment results indicated HepG2 cell survivals might be majorly reduced through mitochondrial apoptosis by DD2. Particularly, p53/Puma is the key signal pathway in intrinsic apoptosis (Wang, et al., 2020). p53 as a tumor suppressor protein related to mitochondrial apoptosis, could transcriptionally activate the p53 upregulated modulator of apoptosis (Puma) in response to various apoptotic stimuli such as DNA damage (Wang, et al., 2020). After Puma activation, it inactivates antiapoptotic Bcl-2 proteins by direct binding, subsequently activated Bax which formed oligomer channels in the mitochondrial membrane, resulting in the increase of MOMP (Chen et al., 2018) and mitochondrial dysfunction. Increased MOMP contributed to the release of cytochrome *c* from mitochondria to the cytosol, leading to the caspase activation cascade. Apoptosis induction was finally performed by increasing the expression of the critical apoptotic marker caspase-3 (He, et al., 2019). In order to elucidate the role of DD2 played in this pathway, effects of DD2 on the major members of mitochondrial apoptosis-related proteins were examined by western blotting. Compared with the control group, the expressions of p53, Puma, Bax, caspase 3 and cleaved-caspase 3 were concentration-dependently upregulated by DD2 (Fig. 6). Simultaneously, the expressions of Bcl-2 were down regulated significantly in a dose-dependent manner (Fig. 6). These results implied that mitochondrial apoptosis induction by DD2 might be conducted through the p53-Puma-Bcl-2/ Bax axis.

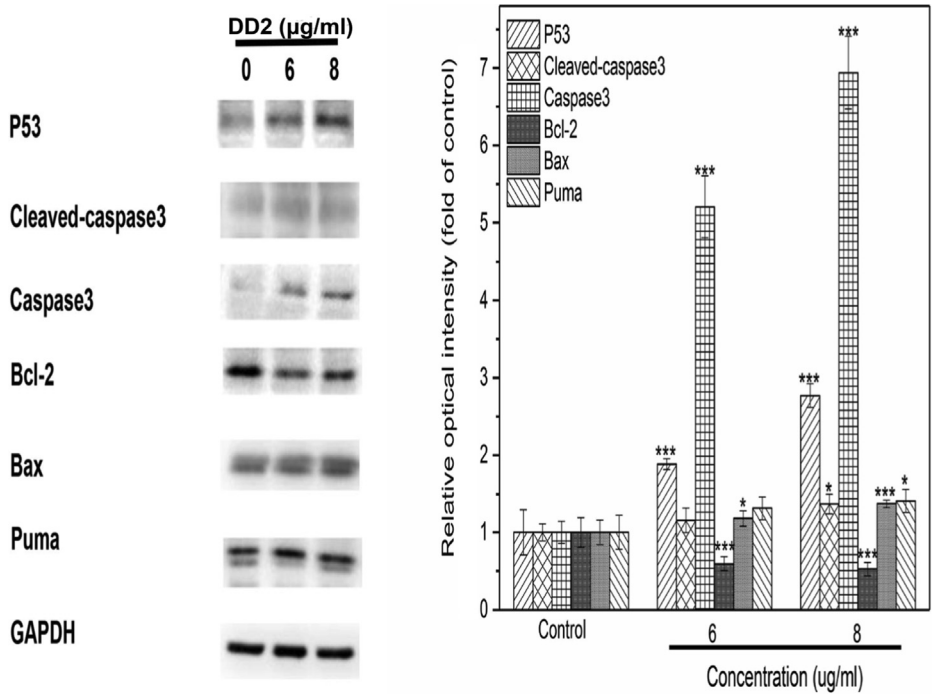

Fig. 6 Results of western blot. HepG2 cells were treated by DD2 with different concentrations for 24 h. Data represent the mean ± SD of three independent experiments. *P < 0.05,***P < 0.001 *vs* untreated control cells.

3.10. DD2 highlighted good antitumor efficacy in vivo

A HepG2 xenograft tumor model using BALB/c nude mice was established to evaluate the antitumor activity of DD2 in hepatocarcinoma *in vivo*. DD2 and PTX at the given dosage significantly suppressed tumor growth, as tumor weights and sizes in these groups were obviously smaller than those of the PBS group on day 16 (Fig. 7a-b). Especially, the fact that DD2 group exhibits an inhibition ratio of ~ 82.1%, which is 1.43 fold of PTX group (Fig. 7c), is consistent with the result of cytotoxicity *in vitro*. Apoptotic cells in tumors from different groups were investigated through the TUNEL assay, showing DD2 and PTX groups induced apparently more TUNEL-positive cells in tumors than PBS group whereas more apoptotic cells were observed after treatment with DD2 (Fig. 8a). This indicated that DD2 produced the superior anticancer efficacy by causing more apoptotic cells in tumors. To further elucidate the mechanism of DD2 inducing tumor apoptosis *in vivo*, immunohistochemistry (ICH) was employed to evaluate the expressions of representative tumor progression markers such as p53, Bax and Bcl-2 in the tumors. Results showed that Bcl-2 was decreased while Bax and p53 were increased in the DD2 or PTX groups in comparison to controls (Fig. 8b), which was in good agreement with *in vitro* cell research results that mitochondrial apoptosis is involved.

Alpha-fetoprotein (AFP) is the crucial tumor marker in the diagnosis and treatment of hepatocarcinoma, which could modulate cell proliferation, cell cycle, apoptosis and migration (Kojima et al., 2011; Yamamoto et al., 2010). Overexpressed AFP should be found in the majority of patients with hepatocarcinoma (Lin et al., 2020), resulting in a poor prognosis by suppressing autophagy and apoptosis and promoting cell growth, migration and invasion (Wang et al., 2018). Serum AFP level of mice in different groups was measured to examine the therapeutic effect of related drugs. As displayed in Fig. S22, the AFP level of mice in PBS group (21.99 ± 2.31 ng/ml) was significantly higher than that in healthy group (10.81 ± 1.12 ng/ml) and DD2 or PTX significantly reduced AFP in serum of tumor-bearing mice (21.99 ± 2.31 *vs* 14.42 ± 0.35 ng/ml; 21.99 ± 2.31 *vs* 14.71 ± 0.75 ng/ml), prompting DD2 might induce tumor cell apoptosis *in vivo* by suppressing AFP expression and the health of tumor-bearing mice improved after DD2 treatmentn (Kojima et al., 2011; Yamamoto et al., 2010).

For safety consideration, the toxicity of DD2 and PTX was evaluated by the analysis of body weight, liver and kidney function, and the histological changes of major organs after treatment. The typical biochemical markers of the liver (AST, ALT, TBIL) and kidney (Cr, BUN) were significantly increased after tumorigenesis in mice (Table S4), indicating the occurrence of abnormal liver and kidney function in mice caused by tumor. Compared with the saline group, these markers of mice treated with DD2 or PTX were significantly decreased (Table S4) due to the therapeutic effect of drugs. In addition, no significant body weight loss was observed in the treatment groups (Fig. 7d). Finally, HE staining showed that DD2 treatment did not induce obvious necrosis in comparison to the controls; on the contrary, PTX induced obvious histopathologic changes in the heart and lung (Fig. 9). These results demonstrated the no/low *in vivo* toxicity of DD2 to mice.

4. Discussion

Pinus koraiensis is large in number and widely distributed, and is the plant resource to be developed urgently (Hou et al.,

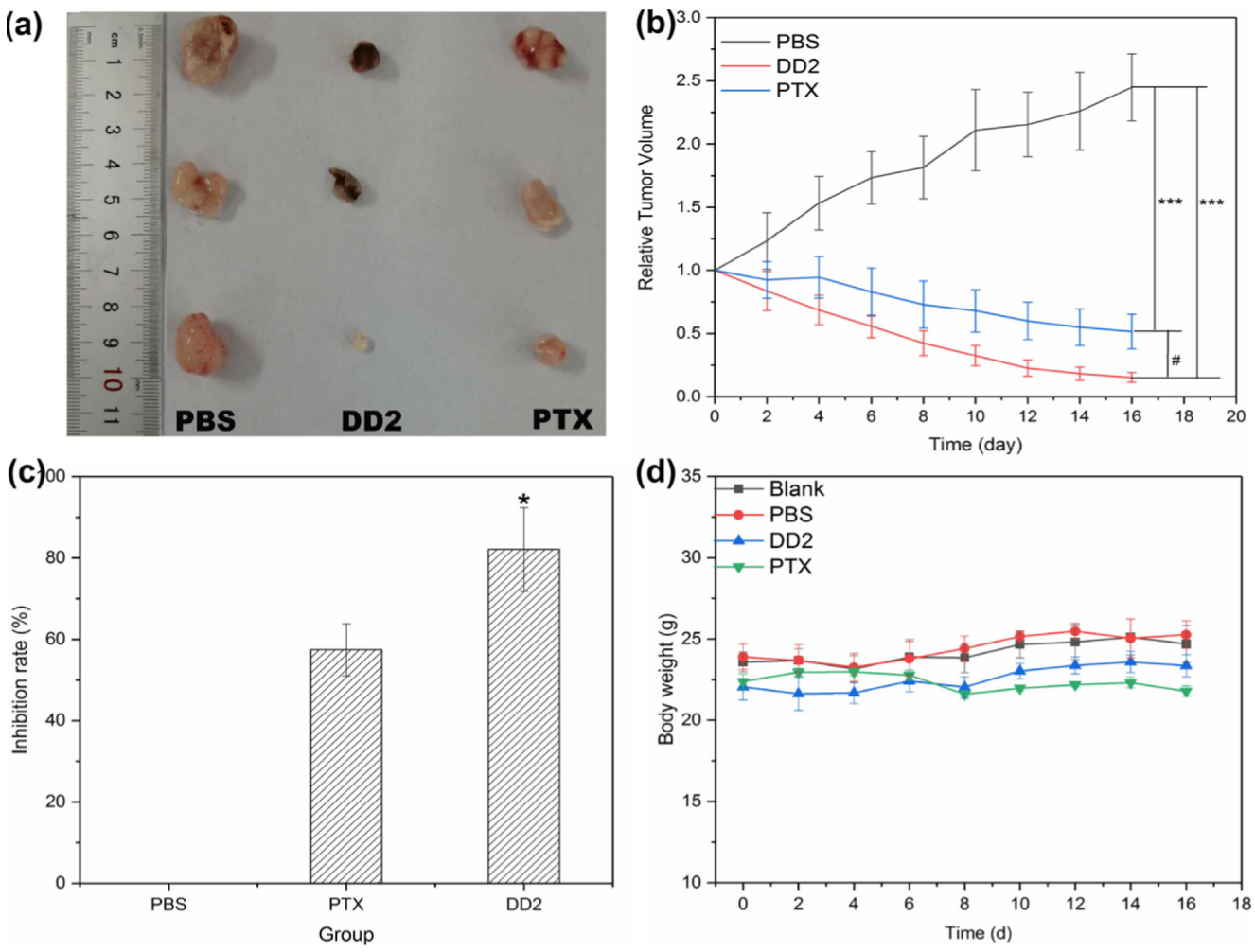

Fig. 7 DD2 inhibited the growth of HepG2 xenograft tumors in nude mice. a, Tumor photo. b, Tumor volume changes of mice treated with DD2, PTX and PBS, respectively. $^{***}P < 0.001$ *vs* control group, $^{\#}P < 0.05$ *vs* PTX group. c, Tumor growth inhibition ratio of the treated mice in different groups. $^{*}P < 0.05$ *vs* PTX group. d, Body weight changes of mice in different treatment groups within 16 d. Data represent the mean ± SD of three independent experiments.

2019). Extracts of *Pinus koraiensis* pinecones could effectively suppress the proliferation of multiple tumor cells and some chemical components including polyphenol, polysaccharide, terpene might be the antitumor efficacy of pinecones (Yi et al., 2015; Lee et al., 2018; Zou et al., 2013). Unfortunately, its exact antitumor efficacy material basis still remained ambiguous. Particularly, 60% ethanol extract from *Pinus koraiensis* pinecones has been found as the active site (Yi et al., 2015; Yi et al., 2016). Therefore, various separation and purification methods were successively adopted along with cellular viability to discover compounds against HepG2 cells (Fig. 10). After identification by HPLC-Orbitap Fusion MSMS and NMR, five compounds (Co.1–5) belonging to abietane diterpenoids (Fig. S4) were obtained. Compounds with different substituents all exhibited strong cytotoxicity to HepG2 cells, indicating tricyclic diterpene structure played an important role in exerting the efficacy. Interestingly, the cytotoxicity caused by compound monomers (Co.1, 2, 4, 5) was lower than that of their mixture. The resulting CI of the related mixture was 0.63 (CI < 1), prompting Co.1, 2, 4, 5 exerted synergistic anticancer effect and their mixture was the "same breath, common destiny" system instead of simple physical superposition of drugs. Certainly, further exploration is necessary to reveal the synergistic antitumor mechanism of these compounds.

Dehydroabietic acid and its derivatives were speculated to be responsible for the antitumor activity in *Pinus koraiensis* pinecones, however, some defects still existed. Firstly, insufficient efficacy of monomeric compounds might result in repeated and high-dose administration; Secondly, the anticancer effect of combining multiple monomers was superior to that of each monomer, with the lack of the efficient multicomponent drug delivery system (the nano drug delivery system that can simultaneously carry multiple compounds with different properties). Recently, cytotoxicity of dehydroabietic acid on tumor cells has been significantly enhanced by chemical grafting nitrogen-containing and aromatic groups on it, indicating chemical modification of tricyclic diterpene structure is an important way to improve the antitumor activity of dehydroabietic acid (Huang et al., 2015; Wang et al., 2016). But in these chemical reactions with cumbersome steps and harsh conditions, structural modification was limited to

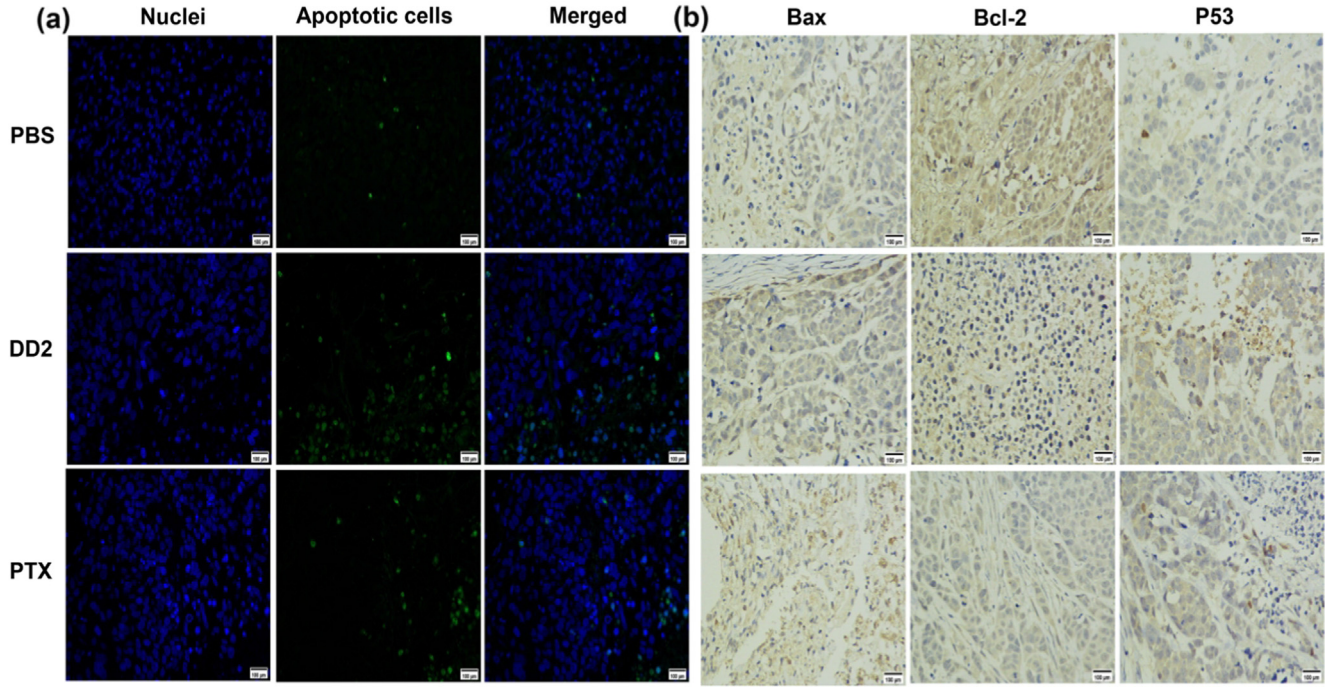

Fig. 8 a, TUNEL images of apoptotic cells in tumor tissue from different treatment groups. Green represents the DNA strand breaks of the apoptotic cells. b, Expression of Bax, Bcl-2 and p53 in xenograft tumors were analyzed by immunohistochemistry. Magnification: × 400, scale bar: 100 μm.

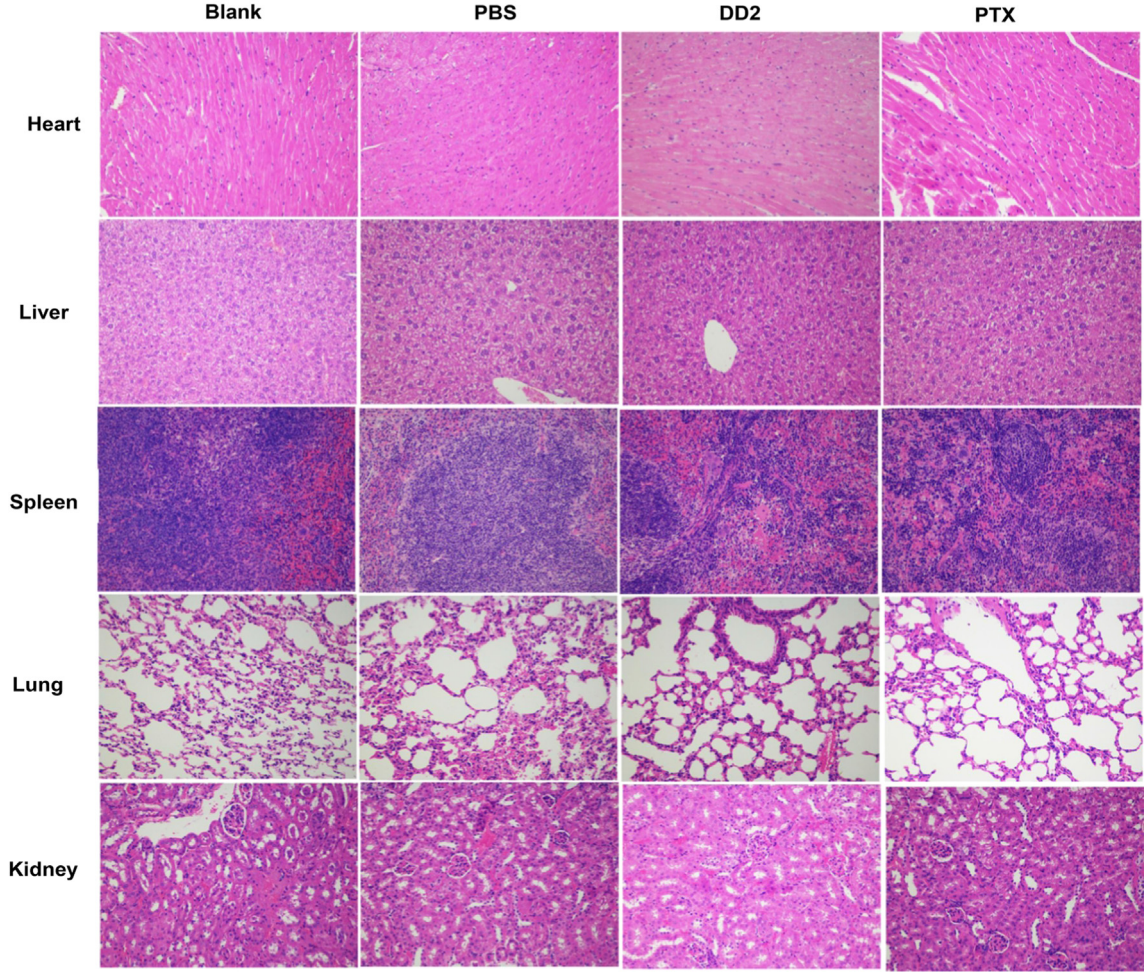

Fig. 9 Histological analysis of major organs from mice in different groups.

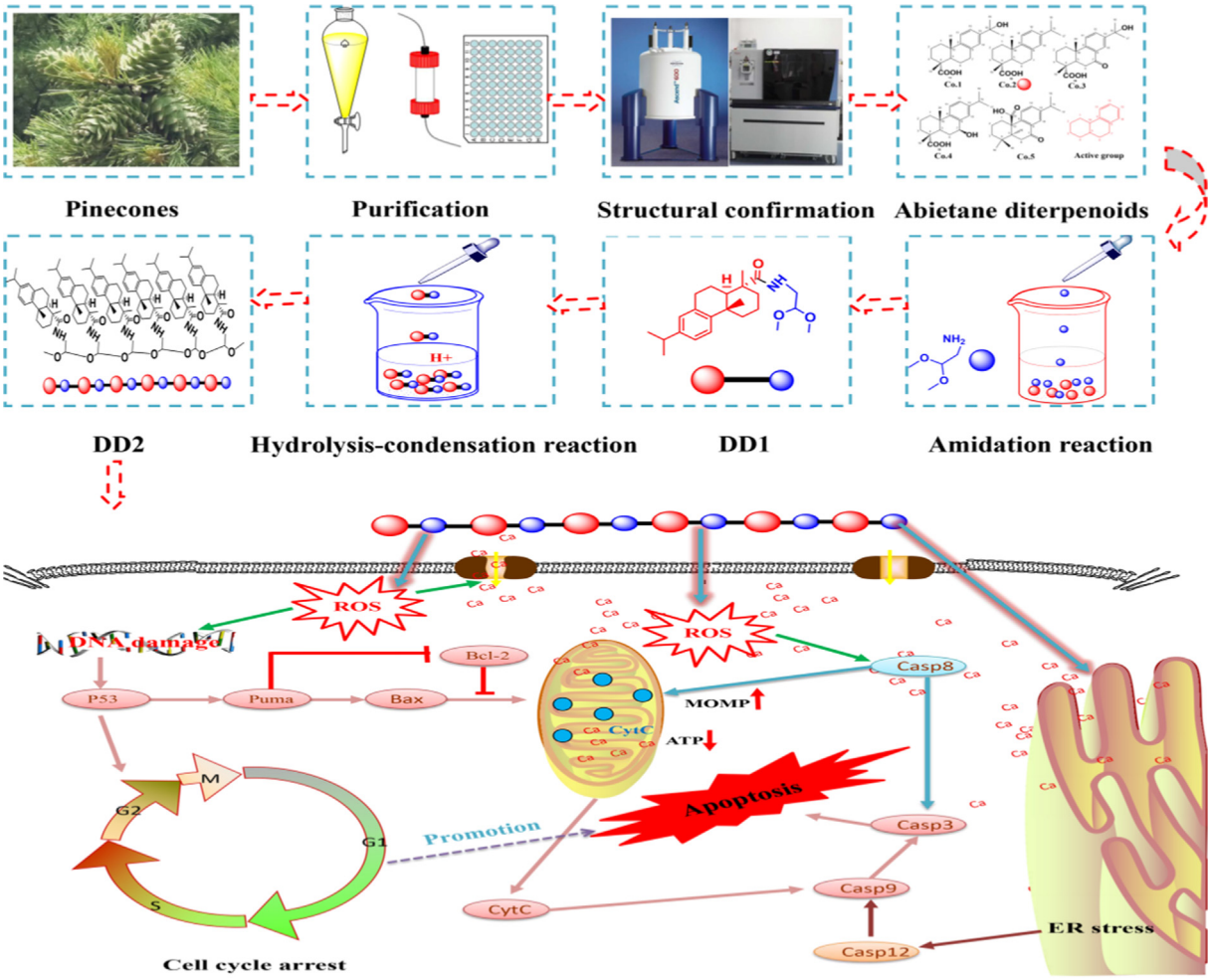

Fig. 10 Flowchart of this study.

the addition of groups on the rings. We speculated that polymerization of multiple tricyclic skeletons should lead to the enhancement of the cytotoxicity against HepG2 cells, based on the fact that tricyclic diterpene is the active core. Therefore, the hexamer of dehydroabietic acid was synthesized through the simple two-step reaction under mild conditions (Fig. 10). Indeed, the hexamer of dehydroabietic acid demonstrated strong antiproliferative activities on hepatoma cells, confirming the feasibility of this simple but efficient strategy. Next, sequential follow-up experiments should be conducted to explore factors affecting the degree of polymerization (DP) such as steric hindrance, water content, reaction time (Zheng et al., 2013) and the relationship between DP and antitumor activity.

Dehydroabietic acid and its derivatives as the novel class of antineoplastic agents could effectively inhibit cell migration, induce cell cycle arrest and block angiogenesis, most importantly, they efficiently trigger apoptosis through both extrinsic and intrinsic apoptosis signal pathway (Lee et al., 2017; Lee et al., 2018; Huang et al., 2015; Wang et al., 2016). Mechanisms of apoptosis induced by DD2 were revealed *in vitro* and *in vivo*. Results *in vitro* suggested three typical apoptotic pathways (extrinsic, intrinsic and endoplasmic reticulum stress-mediated apoptosis signal pathway) were all involved in the process of apoptosis caused by DD2. Given that the three pathways are closely linked, and they could converge on the mitochondrial apoptosis pathway (Yapasert et al., 2020), the intrinsic one was more thoroughly studied. The general process of apoptosis has been summarized as follows (Fig. 10): a. DD2 elevated the intracellular ROS and futher caused the DNA damage; b. DNA damage signal induced cell cycle arrest and activated p53-Puma-Bcl-2/Bax pathway, facilitated the increase of MOMP and caspase activation cascade to trigger the final apoptosis; c. Calcium ion leakage from endoplasmic reticulum and calcium influx induced by ROS resulted in intracellular calcium overload to increase MOMP and activate caspase cascade; d. DD2 directly activated caspase 8 and caspase 12, causing ER stress and extrinsic apoptosis. Furthermore, the anti-tumor activity and safety of DD2 *in vivo* were evaluated based on a HepG2 xenograft tumor model. Given the poor solubility of DD2, intratumoral administration which was safer and more effective than systemic administration was adopted (Park, et al., 2018). Similar to the antitumor results *in vitro*, DD2 could still effectively induce tumor cells apoptosis *in vivo* through the mitochondrial apoptosis pathway with reliable safety, suggesting DD2 might be the effective and safe antineoplastic agent. Importantly, the novel nano drug-delivery system suitable for DD2 and precise

antitumor mechanisms of DD2 are currently under investigation.

5. Conclusion

In general, synergistic antitumor abietane diterpenoids are mainly responsible for the efficacy of 60% ethanol extract from *Pinus koraiensis* pinecones, and their antitumor activities could be significantly enhanced through the polymerization of multiple tricyclic skeletons. Research on the mechanisms implied the hexamer of dehydroabietic acid (DD2) suppressed cell proliferation through cell cycle arrest and promoted apoptotic death by activating three types of typical apoptotic pathways *in vitro*, similarly, DD2 could efficiently induce apoptosis of tumor cells *in vivo* through the mitochondrial apoptosis pathway.

6. Ethics statement

The animal experiments part of this research was approved by the experimental animal welfare ethics committee of Harbin Institute of Technology (IACUC-2019021).

Declaration of competing interest

The authors declare no conflict of interest. All authors agree to submit the manuscript.

Acknowledgements

The authors are grateful to engineer Shu-Mu Li (Institute of Chemistry, Chinese Academy of Sciences) for his kind help of HPLC-Orbitap Fusion MSMS.

Funding

This work was supported by the thirteen five national key research and development projects (Grant No. 2016YFC0500307-07).

Appendix A. Supplementary data

Supplementary data to this article can be found online at https://doi.org/10.1016/j.arabjc.2021.103069.

References

Cortes, J., Perez-García, J.M., Llombart-Cussac, A., et al, 2020. Enhancing global access to cancer medicines. CA Cancer J. Clin., 1–20

IARC, 2020. Latest global cancer data 2020. https://www.iarc.fr/faq/latest-global-cancer-data-2020-qa/ (accessed 4 February 2021).

Batra, H., Pawar, S., Bahl, D., 2019. Curcumin in combination with anti-cancer drugs: a nanomedicine review. Pharmacol Res. 139, 91.

Wei, Q.Y., Xu, Y.M., Lau, A.T.Y., 2020. Recent progress of nanocarrier-based therapy for solid malignancies. Cancers. 12, 2783.

Chung, J.E., Tan, S., Gao, S.J., et al, 2014. Self-assembled micellar nanocomplexes comprising green tea catechin derivatives and protein drugs for cancer therapy. Nature Nanotech. 9, M907–12.

Hou, K., Bao, M., Wang, L., et al, 2019. Aqueous enzymatic pretreatment ionic liquid–lithium salt based microwave–assisted extraction of essential oil and procyanidins from pinecones of Pinus koraiensis. J. Clean. Prod. 236. 117581.

Zhang, Y., Xin, C., Qiu, J., et al, 2019. Essential oil from Pinus koraiensis pinecones inhibits gastric cancer cells via the HIPPO/YAP signal pathway. Molecules 24, 3851.

Yi, J.J., Wang, Z.Y., Bai, H.N., et al, 2016. Polyphenols from pinecones of Pinus koraiensis induce apoptosis in colon cancer cells through the activation of caspase in vitro. RSC Adv. 6, 5278.

Yi, J.J., Cheng, C.L., Li, X.Y., et al, 2017. Protective mechanisms of purified polyphenols from pinecones of Pinus koraiensis on spleen tissues in tumor-bearing S180 mice in vivo. Food Funct. 8, 151.

Yi, J.J., Wang, Z.Y., Bai, H.N., et al, 2015. Optimization of purification, identification and evaluation of the in vitro antitumor activity of polyphenols from Pinus koraiensis pinecones. Molecules 20, 10450–10467.

Li, Z.L., Liu, J., Hu, Y., et al, 2016. Multimodal imaging-guided antitumor photothermal therapy and drug delivery using bismuth selenide spherical sponge. ACS Nano. 10, 9646–9658.

Wang, J.K., Guo, Q., Zhang, X.W., et al, 2020. Aglaia odorata Lour. extract inhibit ischemic neuronal injury potentially via suppressing p53/Puma-mediated mitochondrial apoptosis pathway. J. Ethnopharmacol. 248. 112336.

Li, Z.Z., Chen,Y.D., A,T.T., et al., 2019. Nuciferine inhibits the progression of glioblastoma by suppressing the SOX2-AKT/STAT3-Slug signaling pathway. J Exp Clin Canc Res. 38, 139.

Xin, C., Zhang, Y., Wang, Z.Y., 2021. Research progress of existing problems and countermeasures of anticancer components from pinecones of Pinus koraiensis. Sci Tech Food Ind. 42, 344.

Lee, T.K., Roh, H.S., Yu, J.S., et al, 2017. Pinecone of Pinus koraiensis inducing apoptosis in human lung cancer cells by activating caspase-3 and its chemical constituents. Chem. Biodiversity. 14. e1600412.

Liu, C., Zhao, C., Pan, H.H., et al, 2014. Chemical constituents from inonotus obliquus and their biological activities. J. Nat. Prod. 77, 35–41.

Chou, T.C., Motzer, R.J., Tong, Y.Z., et al, 1994. Computerized quantitation of synergism and antagonism of taxol, topotecan, and cisplatin against human teratocarcinoma cell growth: a rational approach to clinical protocol design. J. Natl. Cancer I. 86, 1517–1524.

Rao, X.P., Song, Z.Q., He, L., et al, 2008. Synthesis, structure analysis and cytotoxicity studies of novel unsymmetrically N, N′-substituted ureas from dehydroabietic acid. Chem Pharm Bull. 56, 1575–1578.

Huang, X.C., Wang, M., Pan, Y.M., et al, 2013. Synthesis and antitumor activities of novel a-aminophosphonates dehydroabietic acid derivatives. Bioorg Med Chem Lett. 23, 5283–5289.

Pertino, M.W., Verdugo, V., Theoduloz, C., et al, 2014. Synthesis and antiproliferative activity of some novel triazole derivatives from dehydroabietic acid. Molecules 19, 2523–2535.

Huang, X.C., Wang, M., Wang, H.S., et al, 2014. Synthesis and antitumor activities of novel dipeptide derivatives derived from dehydroabietic acid. Bioorg Med Chem Lett. 24, 1511–1518.

Li, J., Li, Y.M., Shen, L.Q., et al, 2019b. Synthesis and antitumor activity evaluation of dehydroabieticacid sulfonylureas derivatives. Chinese J. New Drugs. 28, 1779.

Duan, J.Y., Shi, J., Ma, X., et al, 2020. Esculetin inhibits proliferation, migration, and invasion of clear cell renal cell carcinoma cells. Biomed Pharmacothe. 125. 110031.

Xu, W., Bo, W., Yang, M., et al, 2017. Tebufenozide induces G1/S cell cycle arrest and apoptosis in human cells. Environ Toxicol Pharmacol. 49, 89.

Takeda, K., Stagg, J., Yagita, H., et al, 2007. Targeting death-inducing receptors in cancer therapy. Oncogene 26, 3745–3757.

Mazumder, S., Plesca, D., Almasan, A., 2008. Caspase-3 activation is a critical determinant of genotoxic stress-induced apoptosis. Methods Mol. Biol. 414, 13–21.

Garrido, C., Galluzzi, L., Brunet, M., et al, 2006. Mechanisms of cytochrome c release from mitochondria. Cell Death Differ. 13, 1423.
Magalhaes-Novais, S., Bermejo-Millo, J.C., Loureiro, R., et al, 2019. Cell quality control mechanisms maintain stemness and dierentiation potential of P19 embryonic carcinoma cells. Autophagy. 1.
Breckenridge, D.G., Germain, M., Mathai, J.P., et al, 2003. Regulation of apoptosis by endoplasmic reticulum pathways. Oncogene 22, 8608.
Giacomello, M., Drago, I., Pizzo, P., et al, 2007. Mitochondrial Ca2 + as a key regulator of cell life and death. Cell Death Differ. 14, 1267.
Yapasert, R., Sripanidkulchai, B., Teerachaisakul, M., et al, 2020. Anticancer effects of a traditional Thai herbal recipe Benja Amarit extracts against human hepatocellular carcinoma and colon cancer cell by targeting apoptosis pathways. J. Ethnopharmacol. 254. 112732.
Giorgi, C., Baldassari, F., Bononi, A., et al, 2012. Mitochondrial Ca2 + and apoptosis. Cell Calcium 52, 36.
Chen, J.F., Zhong, J.C., Liu, Y.Y., et al, 2018. Purified vitexin compound 1, a new neolignan isolated compound, promotes PUMA-dependent apoptosis in colorectal cancer. Cancer Medicine. 7, 6158.
He, S.F., Ma, X., Ye, Y., et al, 2019. HEATR1 modulates cell survival in non-small cell lung cancer via activation of the p53/PUMA signaling pathway. Oncotargets Ther. 12, 4001.
Kojima, K., Takata, A., Vadnais, C., et al, 2011. MicroRNA122 is a key regulator of alpha-fetoprotein expression and influences the aggressiveness of hepatocellular carcinoma. Nat. Commun. 2, 338.
Yamamoto, K., Imamura, H., Matsuyama, Y., et al, 2010. AFP, AFP-L3, DCP, and GP73 as markers for monitoring treatment response and recurrence and as surrogate markers of clinicopathological variables of HCC. J. Gastroenterol. 45, 1272.
Lin, Y.H., Wu, M.H., Huang, Y.H., et al, 2020. TUG1 Is a regulator of AFP and serves as prognostic marker in non-hepatitis B non-hepatitis C hepatocellular Carcinoma. Cells. 9, 262.
Wang, S., Zhu, M., Wang, Q., et al, 2018. Alpha-fetoprotein inhibits autophagy to promote malignant behaviour in hepatocellular carcinoma cells by activating PI3K/AKT/mTOR signalling. Cell Death Dis. 9, 1027.
Lee, T.K., Park, J.Y., Yu, J.S., et al, 2018. 7a,15-Dihydroxydehydroabietic acid from Pinus koraiensis inhibits the promotion of angiogenesis through downregulation of VEGF, p-Akt and p-ERK in HUVECs. Bioorg. Med. Chem. Lett. 28, 1084.
Zou, P., Yang, X., Huang, W.W., et al, 2013. Characterization and Bioactivity of Polysaccharides Obtained from Pine Cones of Pinus koraiensis by GradedEthanol Precipitation. Molecules 18, 9933.
Huang, X., Huang, R., Liao, Z., et al, 2015. Synthesis and pharmacological evaluation of dehydroabietic acid thiourea derivatives containing bisphosphonate moiety as an inducer of apoptosis. Eur. J. Med. Chem. 108, 381.
Wang, Y.Y., He, Y., Yang, L.F., et al, 2016. Synthesis of novel diterpenoid analogs with in-vivo antitumor activity. Eur. J. Med. Chem. 120, 13.
Zheng, Y.Y., Tang, Q., Wang, T.F., et al, 2013. Synthesis of a green fuel additive over cation resins. Chem. Eng. Technol. 36, 1951.
Park, C.J., Hartl, C.A., Schmid, D., et al, 2018. Extended release of perioperative immunotherapy prevents tumor recurrence and eliminates metastases. Sci. Transl. Med. 10, 1916.